Cement & Concrete Composites 33 (2011) 389–401

Contents lists available at ScienceDirect

Cement & Concrete Composites

journal homepage: www.elsevier.com/locate/cemconcomp

Ultrasonic monitoring of capillary porosity and elastic properties in hydrating cement paste

Xiaojun Wang, Kolluru V. Subramaniam *

City College/City University of New York, Civil Engineering, Rm 110, Steinman Hall, New York, NY 10031, United States

ARTICLE INFO

Article history:
Received 23 July 2009
Received in revised form 8 November 2010
Accepted 10 November 2010
Available online 16 November 2010

Keywords:
Capillary porosity
Ultrasonic
Shear modulus
Hydration
Early-age
Poro-elastic

ABSTRACT

A test procedure for monitoring changes in the amplitude of horizontally polarized ultrasonic shear waves from the surface of hydrating cement paste is presented. A theoretical framework based on a poro-elastic idealization of the hydrating cement paste is developed for interpreting the ultrasonic reflection data. The poro-elastic representation of hydrating cement paste is shown to provide simultaneous, realistic estimates of porosity and shear modulus for hydrating cement paste through setting and early strength gain. The porosity predicted by the poro-elastic representation is identical to the capillary porosity predicted by Powers' model. The shear modulus of the poro-elastic skeleton was found to agree favorably with the value of shear modulus obtained from a vibration-based measurement. Data from cement paste with different water-to-cement ratios indicates a very non-linear relationship between capillary porosity and shear modulus. While there is a steady decrease in the porosity in the first 24 h, there is initially an exponential increase in the shear modulus up to the end of the acceleration period, which is followed by a period with a slower rate of increase.

1. Introduction

In the first few hours after mixing cement and water there are significant changes in the microstructure, which influence property development in the material. Determination of the changes in the microstructure and elastic properties of hydrating cement through setting, and early strength gain of the material has remained a major experimental challenge. Applying conventional methods for studying changes in microstructure in the first few hours after casting are challenging because (a) sample preparation procedures either alter or disturb the microstructure [1,2]; and (b) changes in microstructure in the hydrating system occur on a time scale that is an order of magnitude faster than the time required for sample preparation [3].

Porosity of cement paste is one of the most important microstructural features, which manifests at different length scales. The capillary porosity is associated with the larger length scale, while the gel pores are finer. The volume of porosity has been measured using gas sorption, solvent exchange and thermogravimetric methods [4]. From the measurements of the evaporable and non-evaporable water contents in the cement paste, the degree of hydration and porosity are estimated using relations which are based on known reaction stoichiometry and volumetric proportions of the reaction products [5–7]. The sample preparation required for any of these techniques involves drying and does not permit real-time estimation of porosity changes. Recently, techniques based on small angle scattering (SAS) have been applied to study the development of porosity. Small angle neutron scattering (SANS) and small angle X-ray scattering (SAXS) allow for porosity measurements at the nano-scale and can be used on wet samples without the need for drying. The interpretation of the microstructure of a complex system such as cement paste from the SAS data requires the use of microstructure models for obtaining the relevant quantitative parameters [8].

Different aspects of the pore structure development have been assessed by assimilating information from different techniques. For instance, early age evolution of porosity and changes in the density of the hydration products, have been estimated from the measurement of chemical shrinkage, isothermal calorimetry and imaging [9]. The evolution of the pore connectivity was inferred from electrical measurements by relating the measured bulk electrical conductivity to the pore solution conductivity and porosity, which was obtained from weight loss measurements [10]. It is shown that there are significant changes in the pore connectivity within the first 24 h, which is prominent for low water-to-cement ratios. Experimental investigation of pore structure of hydrating cement paste using scanning electron microscopy and low temperature calorimetry revealed significant changes in the capillary pore system within the first few days of hydration, while the gel pores system is shown to develop later [11]. Changes in the pore structure have been shown to have a significant influence on the

* Corresponding author. Tel.: +1 212 650 6569; fax: +1 212 650 6965.
E-mail address: ksubram@ce.ccny.cuny.edu (K.V. Subramaniam).

0958-9465/$ - see front matter © 2010 Elsevier Ltd All rights reserved.
doi:10.1016/j.cemconcomp.2010.11.001

mechanical properties. The capillary porosity in particular is associated with changes in the mechanical properties, while the finer gel pores influence properties such as shrinkage and creep [2]. Currently a tool for simultaneously monitoring the evolution of porosity and elastic properties of cement paste, which provides non-invasive, real-time assessment, is not available.

The development of microstructure in hydrating cement pastes, especially in the early ages has been simulated using computer models, which indicate that initially starting from a weak skeleton composed of loosely connected cement grains within the fluid medium, the products of hydration link up to provide a continuous network of hydration products within the fluid-filled space [12,13]. The emergence of a continuous solid phase within the fluid medium has been identified as the percolation threshold [12,14,2]. Following the percolation threshold, setting behavior is initiated in the cement paste. Through setting, as the products of hydration form within the fluid-filled spaces of cement paste, a network of pores and a pore structure develops. Successful implementation of the computer models requires calibration of semi-empirical parameters for any given cement.

An ultrasonic technique and data interpretation for continuous simultaneous monitoring of changes in the porosity and elastic material properties in hydrating cement paste are presented in this paper. The primary focus of the research presented here is to assess changes in the microstructure associated with porosity of a hydrating cement paste through the setting process from ultrasonic measurements. The ultrasonic reflection method comprises measuring the changes in the amplitude of a horizontally polarized shear wave (SH waves) at the interface between a buffer plate and the hydrating cement paste. Reflected shear waves have previously been used for studying the setting behavior and evolution of visco-elastic material properties of hydrating cement paste [15–17]. Changes in reflected waves also provide a favorable prediction for strength gain in concrete [18]. An improved test system, with the capability of collecting wave reflection measurements at multiple angles of incidence, is presented. The measured wave response is related to the changes in the microstructure of hydrating cement paste using a poro-elastic representation of cement paste. A poro-elastic equivalent material for hydrating cement paste is derived by matching the measured reflections response with changes in the poro-elastic parameters. The results of the study show that the porosity of the equivalent poro-elastic material compares favorably with the capillary porosity obtained from thermogravimetric measurements by the application of Power's model [6,7]. In addition, the shear modulus of the hydrating cement material obtained from the poro-elastic equivalent is shown to compare favorably with the value obtained from a vibration-based measurement. The method presented here allows for real-time assessment of capillary porosity and shear modulus in hydrating cement paste.

2. Background

The microstructure of hydrating cement can be idealized as a water-filled porous skeleton with evolving porosity and skeleton properties. Previous experimental investigation had revealed that even initially after mixing, cement paste has sufficient structural integrity within the arrangement of cement grains to transmit low magnitude shear stress through the material [19]. At low amplitude shear stress, the freshly mixed cement paste behaves as a weak porous skeleton composed of grains of cement. With time, the cement grains form a three-dimensional network where all grains are continuously connected to the adjacent grains with products of hydration [12,13,19]. On a representative scale, the solid skeleton of cement paste consists of unhydrated cement and the hydration products.

The poro-elastic representation of the microstructure of hydrated cement paste has been found suitable for the microstructure of cement paste at different length scales [20–23]. The mechanical properties at a given length scale have been derived from the properties of components at a lower length scale using homogenization techniques [21]. Using a poro-elastic representation for microstructure of hardened cement paste, the volumetric changes associated with shrinkage have been predicted [20,22,23]. The poro-elastic theory developed by Biot has also been updated to account for partial saturation of the medium to account for drying [24].

In this paper, the poro-elastic representation developed by Biot is used to interpret the wave propagation in hydrating cement paste [25,26]. According to Biot's theory, the volume fraction of the fluid within a unit volume of the material is referred to as the porosity. It is implicitly assumed that the pore size is concentrated around its average value. The pore structure is assumed to be composed of inter-connected void space, which allows relative motion between the fluid of known viscosity and the solid. The porous solid and the solid–fluid system are assumed to be statistically isotropic [25]. The propagation of waves in the fluid-saturated poro-elastic medium depends upon the internal system variables which are the effective elastic properties of the porous solid, the porosity, and the parameters related to the pore structure, which influence the relative local movement between the fluid and the solid [25–27].

Considering Biot's poroplastic idealization for hydrating cement paste, the solid skeleton at any given time is assumed to be composed of the products of hydration and the unhydrated cement. The porosity would be three-dimensional water-filled pore space within the skeleton. The disconnected pore space, if any, forms a part of the solid skeleton and it influences the effective materials properties of the skeleton. The fraction of total volume occupied by water within connected pores is the porosity, which is assumed to be isotropic on a representative length scale.

The basic equations for wave propagation in a poro-elastic medium are presented in Appendix A. The solutions for these equations have been worked out by several researchers [27–29]. Three distinct modes of wave propagation including two compression waves and a single shear wave have been shown for a fluid-filled porous medium [30]. For the case of the compression wave, the solution for reflection at the interface between a fluid/elastic material and a porous medium has been determined previously [27,31]. Using a similar procedure, the reflection coefficient, $r^*(f)$, for a horizontally polarized shear wave reflected at the interface between an elastic material and a porous medium, with consideration of a specific set of boundary conditions [32,33], can be derived as (see derivation in Appendix A)

$$r^*(f) = \frac{\bar{\mu}_b k^*_{sh} \cos(\alpha) - \mu_1 k_1 \cos(\theta)}{\bar{\mu}_b k^*_{sh} \cos(\alpha) + \mu_1 k_1 \cos(\theta)} \tag{1}$$

where $\bar{\mu}_b$ is the complex dynamic bulk shear modulus of the solid skeletal frame of the porous medium, μ_1 is the shear modulus of elastic material, k^*_{sh} (complex) and k_1 are the wave numbers in the porous medium and the elastic material, respectively, θ is the angle of incidence and α (complex) is the angle associated with the refracted wave. It should be noted that wave number in the context of wave propagation is the spatial analog of frequency, and defines the phase change per unit distance travelled by the wave. $\mathrm{Cos}(\alpha)$ can be taken equal to 1.0, when the acoustic impedance of the elastic material is larger than the acoustic impedance of the other material [34].

The reflection coefficient, $r^*(f)$ is a complex number written as

$$r^*(f) = r(f)e^{j\Phi} \tag{2}$$

where $r(f)$ and Φ represent changes in the amplitude and phase of the SH wave following reflection at the cement paste/fused-quartz interface, respectively. The decrease in the amplitude of an incident wave following reflection at the interface depends upon the properties of the porous material in contact with the elastic material. Therefore, changes in the amplitude of the reflected waves with time can be related to changes in the microstructure of the poroelastic material.

3. Experimental program

The test program consisted of the following measurements: (a) ultrasonic SH wave reflection; (b) thermogravimetric weight loss measurements; and (c) vibration measurements. Measurements were primarily performed in the first 24 h after casting. Cement paste samples with different water-to-cement ratios were prepared and tested. The composition of the Type I/II cement used is shown in Table 1. The Blaine fineness of the cement was 390 m^2/kg and the average particle size was 15 μm.

3.1. Sample preparation

Cement paste samples were mixed using a paddle mixer following a procedure suggested by Williams et al. [35], which is similar to ASTM C-305. Cement and water were initially mixed at 140 rpm for 30 s, followed by a pause for 1 min before mixing for another 2.5 min at 285 rpm. Cement paste adhering to the sides of the mixing bowl was scraped and the entire mixture was mixed for another 2.5 min at 285 rpm. Cement paste samples with three different water-to-cement ratios equal to 0.35, 0.45 and 0.5, were evaluated in the test program.

3.2. Ultrasonic SH wave reflection method

The ultrasonic wave reflection experimental system was developed to monitor the SH wave reflection at the interface between a buffer plate and cement paste, at 0°, 50° and 60° angles of incidence. The choice of the angles for reflection measurements is explained in a previous paper [19]. While the 50° and 60° measurements provide higher sensitivity, measurements at normal incidence provided a convenient reference for evaluating changes in the reflected waves. A buffer plate made of fused-quartz with precisely machined faces at matched angles with respect to the vertical was used. Ultrasonic shear-wave transducer(s), with a nominal center frequency of 1 MHz, were attached to the buffer plate using a solid couplant. Normal incidence (0° angle) measurements were performed in the pulse-echo mode, where a single transducer attached on the bottom surface functions as the transmitter as well as the receiver. At each oblique angle of incidence, a matched pair of direct contact transducers mounted on the oppositely-angled surfaces of the fused-quartz plate, functioned as the transmitter and receiver. The transducers were attached precisely at the center of the angled surfaces. While attaching the transducers, the axes of the transducers were aligned to generate a horizontally polarized shear (SH) wave in the fused-quartz.

The experimental system comprised equipment for generating, capturing and digitizing ultrasonic waves and included three pulse receivers, a function generator, an oscilloscope, and a computer. A schematic sketch of the test setup is shown in Fig. 1. Signal generation at each angle of incidence was controlled by one of three separate pulser-receivers and was individually triggered using a timer system at discrete time intervals to ensure that only signals from one angle of incidence were incident at the interface at any given time. The reflected signal detected by the corresponding receiver was digitized by the oscilloscope. The data acquisition and transfer were controlled by the computer over a GPIB interface. The oscilloscope had a digitization rate of 500 MS/s which provides a temporal resolution of 2 ns. The influence of random noise in the signal was minimized by taking an average of 100 waveforms in each acquisition. At each angle of incidence, an averaged waveform was acquired every 30 min. Data collection was switched between the different angles every 10 min allowing sufficient time to take the average and minimize the volume of data collected over a typical monitoring period. The entire system was placed inside an environmental chamber, which was maintained at 24 °C throughout the duration of the test.

A cylindrical sample holder (diameter = 75 mm and height = 100 mm) was attached to the top surface of the fused-quartz plate using silicone. The data collection procedure consisted of collecting reflected ultrasonic waves with an empty sample holder for each angle of incidence. The waves collected from the fused-quartz/air interface were collected and recorded before commencing mixing of cement paste. Immediately after mixing, the cement paste was placed in the sample holder up to approximately half the height. The entire assembly of the fused-quartz and sample holder was gently vibrated to remove any entrapped air. The weight of the fused-quartz plate and sample holder with the cement paste was recorded before initiating the readings. The top surface of the cement paste sample was covered with a moist sponge which filled the remaining space within the sample holder. The top surface of the sample holder was sealed using aluminum tape. The transducers were then connected to the pulser-receivers and the data collection was initiated. At the end of the test, the instrumentation was disconnected and the weight of the fused-quartz plate with sample holder and cement paste sample was recorded. The hardened cement paste was demolded, dried with paper towels and its density was determined using a balance with an accuracy of 0.01 g.

Data processing consisted of determining the change in the amplitude of the incident wave upon reflection at the fused-quart/cement paste interface. The reflection factor, which is the ratio of the reflected wave amplitude to the incident wave amplitude, $r(f)$, was obtained using the self-compensating technique [36]. Using the reflected signal from the fused-quartz/air interface as the reference, $r(f)$ at the cement paste/quartz interface was determined by normalizing the reflected magnitude off the fused-quartz/cement paste interface with the reflected amplitude off the fused-quartz/air interface [36,18,19,15,37]. The time domain signals were transformed to frequency domain using the FFT algorithm and the amplitude reflection factor at 1 MHz, $r(1)$, was determined as the ratio of the respective magnitudes of the FFT of the ultrasonic signals from the quartz/cement paste to the quartz/air interface at that frequency. The $r(1)$ obtained using this procedure corresponds to the change in the amplitude of a wave of 1 MHz frequency upon reflection at the interface between fused-quartz and cement paste.

3.3. Thermogravimetric weight loss measurements

Thermogravimetric weight loss measurements were performed to determine the evaporable and the non-evaporable water contents within the hydrating cement paste at different ages. Cement paste samples for weight loss measurements, were cast inside sealed flexible plastic tubes. At a specified time, the

Table 1
Composition of the Type I/II cement.

SiO_2	Al_2O_3	Fe_2O_3	CaO	MgO	SO_3
20.55	4.57	3.03	63.21	3.02	2.79

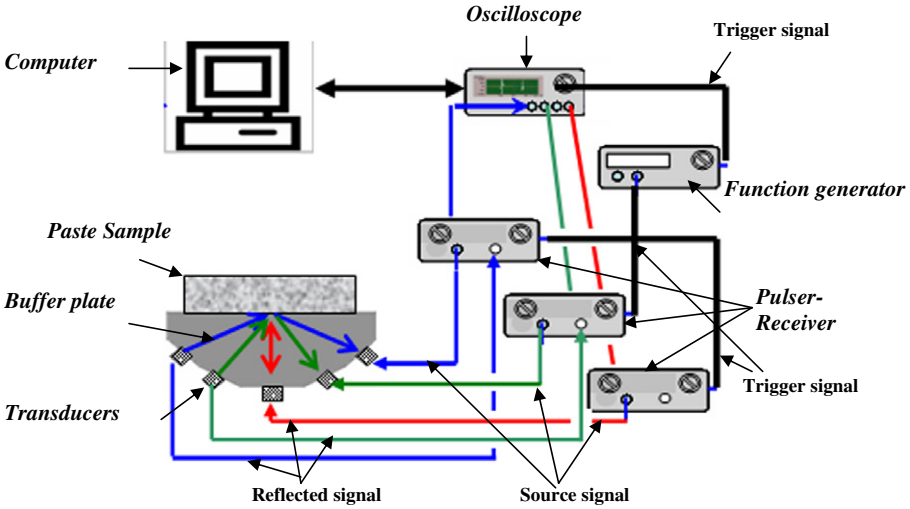

Fig. 1. Schematic of ultrasonic experimental system.

cement paste sample was crushed inside the tube and then extracted by cutting the tube. The extracted sample was then ground using a mortar and pestle and the material passing through a No. 40 sieve was flushed with ethanol in a thistle tube. The sample was then divided into three replicates, approximately 150 mg each and introduced into crucibles of pre-measured weights. A slightly different procedure was followed for the measurements within the first few hours after casting while the cement had not set completely. The paste was extracted from the tube by cutting the tube, spread over the inside surface of the crucible using a spatula, immediately flushed with ethanol, weighed and introduced into a furnace. Weights of the samples were measured with an accuracy of 0.1 mg. The sample preparation was performed under flowing nitrogen gas. The temperature was ramped up to 105 °C in 2 h and held constant. Weights of the samples were recorded after drying the sample at 105 °C before ramping the temperature to 1000 °C at 10 °C/min. During the heating, the furnace was purged with nitrogen gas. The evaporable (w_e) and non-evaporable (w_n) water contents for each crucible were determined. The non-evaporable water content was corrected for the loss on ignition of unhydrated cement powder, which was determined separately [38]. It should be noted that the weight loss measurements at 105 °C do contain contributions from the dehydration of ettringite. The contribution from dehydration of ettringite can be considered to be small considering the sulfate content of cement is low. The degree of hydration, $\alpha_h(t)$ was determined as follows

$$\alpha_h(t) = \frac{w_n(t)/w_{\text{cement}}}{w_{n\infty}/w_{\text{cement}}} \tag{3}$$

where $w_{n\infty}$ is the non-evaporable water content for the complete hydration [5,6], w_{cement} is the weight of cement powder. An approximation for the non-evaporable water for complete hydration, $w_{n\infty}/w_{\text{cement}} \cong 0.23$, obtained by Powers was used. The water-filled porosity at certain degree of hydration then was calculated using the relations presented by Hansen [1986] as

$$\phi(t) = \frac{\rho_{\text{cement}}(w/c) - (1.15 + 0.06\rho_{\text{cement}})\alpha_h(t)}{1 + (\rho_{\text{cement}})(w/c)} \tag{4}$$

where ρ_{cement} is the specific gravity of cement and w/c is the water-to-cement ratio. In subsequent discussion, ϕ refers to water-filled porosity in cement paste.

4. Vibration-based measurement of elastic properties

A vibration-based technique was used to measure the dynamic elastic material constants (Young's modulus and Poisson's ratio) from the longitudinal modes of vibration of cylindrical specimens with length-to-diameter ratio equal to 2.0 [39]. The test setup used for the vibration measurement is shown in Fig. 2. In a typical measurement, the longitudinal vibrations are initiated by the impact of a steel sphere at the center of one end of the cylindrical specimen. The resulting vibrations are monitored using a miniature accelerometer that is mounted at the center of the other end from the impact point. In the experimental setup used in this study, the signal from the accelerometer is acquired by the oscilloscope that is then transferred to a personal computer. The first two longitudinal resonance frequencies of the cylindrical specimen are then picked up from the frequency domain signal obtained from a Fourier transform of the time domain signal. The elastic constants of the cement paste sample are obtained using analytical formulas proposed by Subramaniam et al. [39]. The Poisson's ratio, υ is determined as a function of measured first f_1 and second f_2 longitudinal resonance frequencies as

$$\upsilon = A_1\left(\frac{f_2}{f_1}\right)^2 + B_1\left(\frac{f_2}{f_1}\right) + C_1 \tag{5}$$

where A_1, B_1 and C_1 are functions of the length, L and the diameter, D of the cylinder, given as $A_1 = -8.6457(L/D)^2 + 24.4431(L/D) - 12.4778$, $B_1 = 34.5986(L/D)^2 - 101.7207(L/D) + 56.172$ and $C_1 = -34.6807(L/D)^2 + 105.979(L/D) - 62.731$

Similarly, the shear modulus G is determined as

$$G = \rho\left(\frac{2\pi f_1 R_o}{f_n^1}\right)^2 \tag{6}$$

where ρ is the density of sample, R_o is the radius of cylinder,

$$f_n^1 = A_2(\upsilon)^2 + B_2(\upsilon) + C_2 \tag{7}$$

A_2, B_2 and C_2 are functions of L/D, given as $A_2 = -0.2792(L/D)^2 + 1.4585(L/D) - 2.1093$, $B_2 = 0.0846(L/D)^2 - 0.5868(L/D) + 1.3791$ and $C_2 = 0.285(L/D)^2 - 1.7026(L/D) + 3.3769$.

Cement paste specimens with diameter and length equal to 2 in and 4 in, respectively were cast from the same batch of cement used for ultrasonic and thermogravimetric measurements. The specimens were cast in cylindrical molds and vibrated to remove any entrapped air. The specimens were demolded after 8 h and

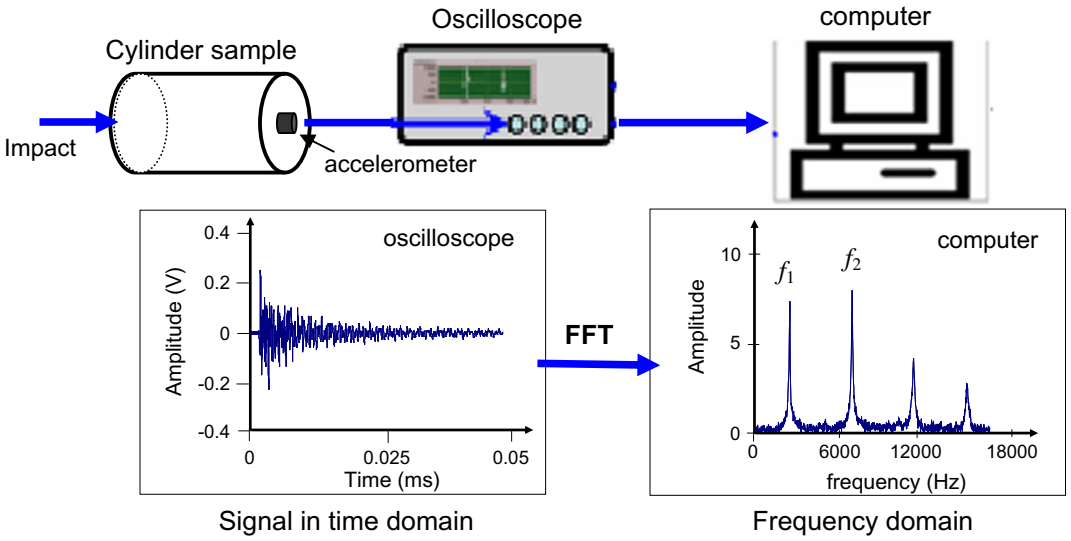

Fig. 2. Schematic of vibration test setup and spectrum.

wrapped in two layers of aluminum tape. Small portions of the circular faces approximately 5 mm × 5 mm in size, centered on the longitudinal axis of the cylinder, were left uncovered by the aluminum tape. These areas were covered using Teflon tape, which could be removed easily. During a measurement these areas, not covered by the aluminum tape, were used for attaching the accelerometer and for the impact point.

5. Experimental results

A typical result of the changes in $r(1)$ at three different angles of incidence for cement paste with w/c ratio of 0.45 is shown in Fig. 3. It can be seen that while the general trends from all three angles of incidence are nominally similar, measurements from larger angles of incidence register a larger magnitude of change at any given time. Initially, the measured $r(1)$ for the three angles of incidence are close to 1.0, suggesting that a significant portion of the incident wave energy is reflected at the quartz/cement paste interface. With time, initially, there is a gradual decrease, which is then followed by a more rapid change in $r(1)$. After approximately 12 h, there is a distinctive change in the rate of decrease in $r(1)$. The changes in temperature recorded from the same sample are also shown in the plot for comparison. The different stages in the hydration reaction can clearly be identified from the temperature profile. The changes in measured $r(1)$ at all three angles of incidence correspond well with the changes in temperature. There is a very rapid decrease in $r(1)$ during the acceleration stage indicated by temperature measurements. There is a distinctive change in the rate of decrease of $r(1)$ associated with the end of the acceleration stage. The measured responses from the other w/c ratios were nominally similar.

The values of Young's modulus ($E = 2G(1 + \upsilon)$) determined from the vibration measurements as a function of time are shown in Fig. 4. For cement paste with $w/c = 0.5$, while readings were initiated for samples after 8 h, no charge was detected in Poisson's ratio until after 10 h. The trends in elastic modulus indicate a very rapid increase in E in the first 24 h, while there an overall decrease in Poisson's ratio with some variation. The results from the different w/c ratios consistently indicate a higher magnitude of E for lower w/c ratio at any given time. It is however interesting to note that there is a larger relative increase in the magnitude of E for the cement paste with a larger w/c ratio.

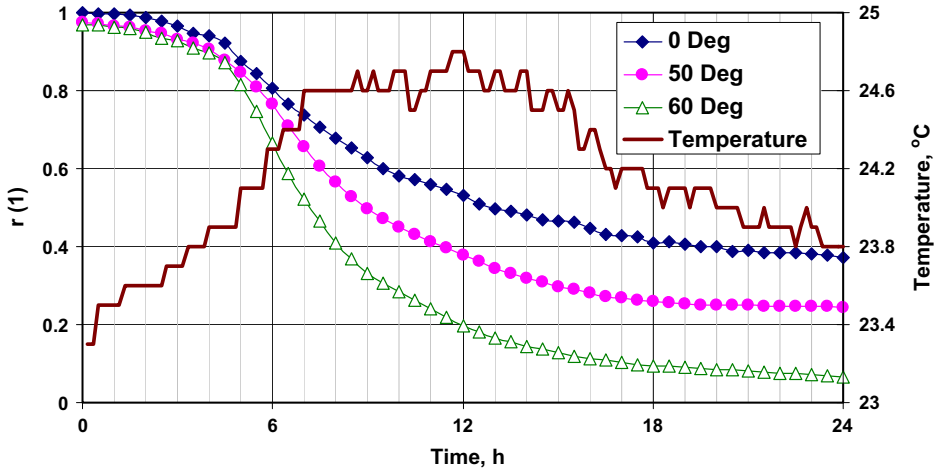

Fig. 3. Evolution of amplitude reflection coefficient for different incident angles.

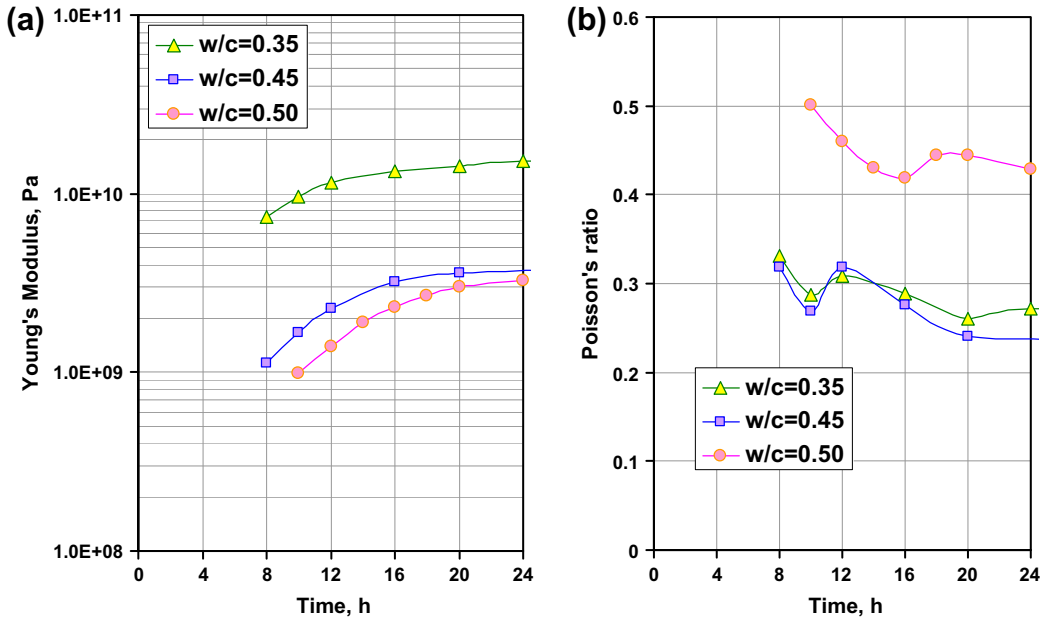

Fig. 4. Vibration measurements as a function of time: (a) Young's modulus; and (b) Poisson's ratio.

The degree of hydration and the changes in porosity of the hydrating cement pastes determined from the thermogravimetric weight loss measurements are shown in Fig. 5. It can be seen that there is a steady decrease in the capillary porosity with an increase in the degree of hydration.

6. Analysis of results

The measured changes in the $r(1)$ at the fused-quartz/cement paste interface can now be interpreted in terms of the expected result from the reflection of an SH wave at the interface between an elastic and a poro-elastic material. The reflection coefficient at the interface, $r(f)$ depends upon the material properties of both media in contact. The functional form of $r(f)$ given in Eq. (8a), can be expressed as

$$r(f) = \left|\frac{\bar{\mu}_b k^*_{sh}\cos(\alpha) - \mu_1 k_1 \cos(\theta)}{\bar{\mu}_b k^*_{sh}\cos(\alpha) + \mu_1 k_1 \cos(\theta)}\right| \tag{8a}$$

where

$$k^*_{sh} = \left[\left(\rho_b\omega^2 - \frac{(\rho_f\omega^2)^2}{m'\omega^2 - j\omega(F\eta/\kappa)}\right)\Big/\bar{\mu}_b\right]^{1/2} \tag{8b}$$

$$F(\omega, c, \eta) = \left(1 + \frac{1}{2}j\omega\frac{\rho_f\kappa c}{\eta\phi}\right)^{1/2} \tag{8c}$$

$$m' = c\rho_f/\phi \tag{8d}$$

$$\rho_b = (1-\phi)\rho_s + \phi\rho_f \tag{8e}$$

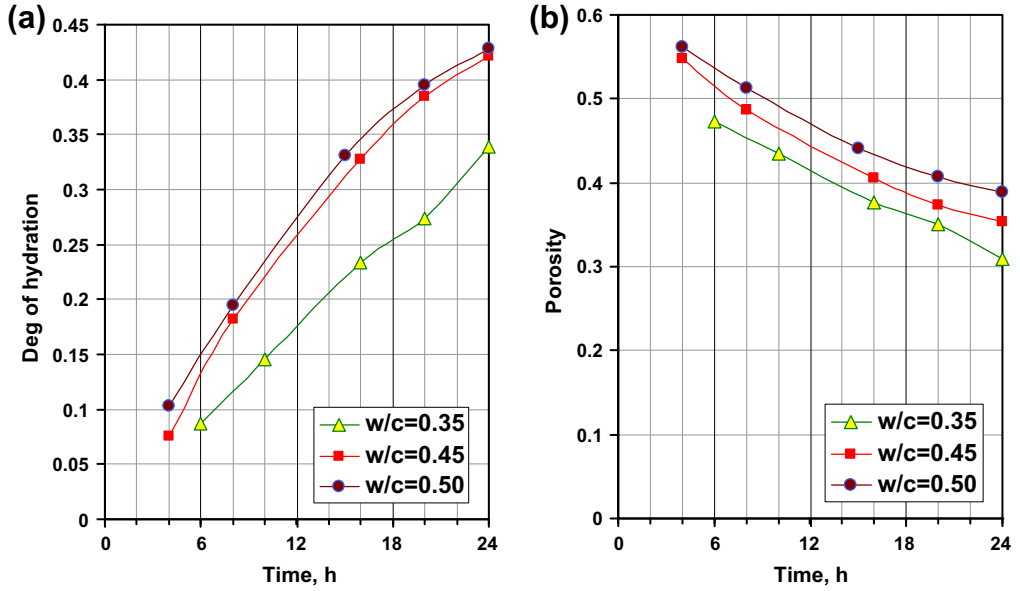

Fig. 5. Thermogravimetric weight loss measurements: (a) degree of hydration; and (b) capillary porosity.

$$\bar{\mu}_b = \mu_b(1 + \delta_\mu j) \tag{8f}$$

$$\mu_1 = \frac{E_1}{2(1+\nu_1)} \text{ and } k_1 = \frac{\omega}{\sqrt{\mu_1/\rho_1}} \tag{8g}$$

ρ_1, E_1, and ν_1 are the density, the Young's modulus and the Poisson's ratio, respectively of the fused-quartz, μ_b and δ_μ are the drained shear modulus of the skeleton and the loss factor, respectively, κ is the permeability of the porous medium, c is the tortuosity of the pore space, η is the viscosity of the fluid, ϕ is the porosity of the poro-elastic medium, ρ_f is the density of the fluid, ρ_s is the density of the skeleton material and ρ_b is the bulk density of the poro-elastic material. A better description of the variables involved is provided in Appendix A. It can be seen that the expression for $r(f)$ does not allow for identifying the explicit functional relationships between the variables and $r(f)$. The function $r(f)$ can however be symbolically expressed as a function R_s, given as

$$r(f) = R_s(\rho_e, E_e, \upsilon_e, \rho_s, \rho_f, K_f, \bar{\mu}_b, \phi, \eta, c, \kappa) \tag{8h}$$

When applied to the case of hydrating cement paste, which is assumed to be a water-filled porous skeleton composed of cement grains and products of hydration, the bulk properties of water are readily available as $K_f = 2.2 \times 10^9$ Pa, $\rho_f = 1 \times 10^3$ kg/m^3 and the viscosity $\eta = 0.9 \times 10^{-3}$ kg/ms.

The analysis can be simplified by considering inter-relations between some of the material parameters, which were introduced by Berryman [40]. The tortuosity, c can be calculated as a function of porosity (ϕ) as

$$c = 1 - s(1 - 1/\phi) \tag{9}$$

where s is a factor, which must be calculated from a microscopic model of the frame moving in the fluid. The value of s equal to ½, which is the exact value for the case of spheres in a fluid medium, was found to provide a reasonable estimate for shear waves in a porous medium [40]. The relationship between permeability, pore size and porosity, given by the Kozeny–Carman relation, was found to be suitable for porous media and is given as

$$\kappa(1-\phi)^2/\phi^3 = \kappa_o(1-\phi_o)^2/\phi_o^3 = \text{const.} \tag{10}$$

and similarly

$$a^2/\kappa = a_o^2/\kappa_o = \text{const.} \tag{11}$$

where a is the pore diameter, ϕ_o, κ_o, a_o are the initial porosity, permeability and pore diameter, respectively. The pore size parameter, a, cannot be measured directly but is estimated to be (1/6–1/7) of the grain size [40]. These inter-relations between some of the parameters of the porous material that were found to provide an accurate description of elastic wave propagation in fluid-saturated porous media such as fine grained sands and sintered porous glass [41,30]. The results were also found to be insensitive to the exact relationships between porosity of the solid and properties which influence bulk flow of the fluid, such as permeability and tortuosity.

Considering the hydrating cement material to be composed of two components, the porous skeleton (made up of cement grains and products of hydration) and water, a simple relation can be obtained considering the relationship for a sealed poro-elastic system given in Eq. (8e). When applied to hydrating cement paste, ρ_s represents the effective density of the solid material composed of the unhydrated cement and the products of hydration, ρ_f is the bulk density of water, and ρ_b is the bulk density of the cement paste. In a sealed system, any changes in ρ_b can only be attributed to changes in volume due to contraction of the bulk. The ρ_b of cement paste samples were measured at 3 days of age and were found to be 2.06, 1.87 and 1.85 g/cm^3, respectively for w/c equal to 0.35, 0.45 and 0.5. These values compare very well with the calculated values of density obtained from the weight proportions of cement paste for a fixed w/c ratio

$$\rho_{\text{cement-paste}} = \frac{1 + w/c}{\frac{1}{\rho_{\text{cement}}} + \frac{w}{c}} \tag{12}$$

Assuming ρ_{cement} is equal to 3.2, the values of $\rho_{\text{cement-paste}}$ are obtained to be 2.055, 1.907 and 1.855 g/cm^3 for w/c equal to 0.35, 0.45 and 0.5, respectively. Thus, for the cement pastes evaluated in this program, ρ_b can be considered to be constant, equal to $\rho_{\text{cement-paste}}$, during the period of observation. The ρ_s, can therefore be obtained using Eq. (8e), further reducing the number of internal variables in the function R_s for $r(f)$.

The material properties of fused-quartz are readily available, further reducing the number of internal variables in the expression in R_s. The reflection at the fused-quartz/cement paste interface can be expressed in terms of the porosity and shear modulus of the skeleton, as

$$r(f) = R_s(\mu_b, \phi, \delta_\mu) \tag{13}$$

In the simplified form, changes in the amplitude of the incident SH wave depend upon three key internal variables of the poro-elastic medium, which are functions of age (time after mixing). Since obtaining analytical expressions for the inversion of the internal variables from the expression for R_s is intractable, numerical inversion was performed to optimize the material constants such that the theoretical prediction is close to the experimental response. The experimental data used in the optimization consists of the $r(1)$ at three different angles of incidence. The generalized reduced gradient non-linear optimization scheme was used to minimize an objective function given as

$$\text{Fun}(c_i) = \sqrt{\frac{\sum_{n=1}^{3}\left(|r(1)|_{\theta_n} - |R_s(\theta_n, c_i)|\right)^2}{3}} \tag{14}$$

where θ_n is the discrete incident angle at which experimental values are obtained, and c_i are the internal system variables of the poro-elastic solid.

For the numerical inversion, the starting guess of porosity for the first measurement after mixing was obtained using the relation

$$\phi_o = \frac{\rho_{\text{cement}}(w/c)}{1 + \rho_{\text{cement}}(w/c)} \tag{15}$$

where ρ_{cement}, the specific gravity of cement, was assumed to be 3.2. The pore size parameter, a_o was taken to be 1/6 of the average cement grain size, which is equal to 2.5 μm. The initial value of permeability, κ_o was estimated using an expression obtained from the application of the general effective medium theory [42]

$$\kappa_o = \frac{l_c^2(1.8)(\phi_o - \phi_c)^2}{226} \tag{16}$$

where ϕ_c is a constant equal to 0.18 and l_c, the critical pore diameter was assumed to be equal to a_o. The starting guess for μ_b was taken as 10^5 Pa. The range for δ_μ was initially prescribed to be within 0.01–0.3. It was found that within the prescribed range, there was an insignificant influence of δ_μ on the final values of μ_b and ϕ. The solution obtained at a given time was used as the starting guess for the next time.

6.1. Evolution of porosity and shear modulus in hydrating cement pastes

The shear modulus and porosity of the cement pastes of three water–cement ratios obtained from the numerical inversion of the test data are shown in Fig. 6. Similar trends in the changes in modulus and porosity for the three mixtures can be observed. It

is interesting to note that there is a continuous increase in the shear modulus after casting, which is almost exponential within the first few hours following which there is a decrease in the rate. The change in the rate of increase of shear modulus corresponds in time with the end of the acceleration period indicated by the temperature measurements. The end of the acceleration period has been associated with a change in the rate controlling mechanism [43]. The change in the rate of modulus increase is therefore indicative of a change to a chemical and diffusion controlled reaction. The porosity obtained from the ultrasonic data corresponds to relative proportion of the water-filled space within a solid skeleton. The measured decrease in porosity is therefore equal to the increase in the solid fraction within the cement paste. Comparing the relative changes in the shear modulus and porosity obtained from the ultrasonic data, it is interesting to note that there is a three order of magnitude increase in the shear modulus corresponding to relatively small change in the porosity. Further there is no significant change in the rate of porosity decrease while the shear modulus exhibits a distinctive change in the rate of increase. There is hence a very non-linear relationship between the decrease in porosity and increase in modulus. Further, there appears to be a larger relative increase in the shear modulus for a given change in the porosity for lower w/c ratio. For a lower w/c ratio, because of the initial closer spacing of cement grains a smaller volume of hydration products produce a higher change in the shear modulus [19].

The measurements on porosity of cement paste obtained from the ultrasonic measurements are compared with the values obtained from the thermogravimetric weight loss measurements (referred to as TGA) in Fig. 7. The porosities obtained from weight loss measurements agree well with the porosities from poro-elasticity based inversion of ultrasonic data. The relationship between porosity and the degree of hydration, given in Eq. (4), was given by Powers and provides an estimate of the capillary porosity in the system. In addition, the values of porosity determined from thermogravimetric measurements for cement paste with w/c equal to 0.5 by Voigt [16,44] are also plotted in the Figure. The close agreement between the values of porosity obtained from the poro-elastic equivalent derived from wave reflection measurements and the capillary porosity calculated by applying Power's model to weight loss measurements provides a validation of the measured porosity. Further, it can be inferred that on the scale of the observation indicated by the ultrasonic waves, the porosity of the equivalent water-filled poro-elastic material corresponds with the capillary porosity within the hydrating cement paste.

The shear modulus of solid skeleton from ultrasonic data is compared with the shear modulus obtained from the vibration test as shown in Fig. 8. It should be noted that while there is a good agreement between the trends and the values of shear moduli derived from the two measurements, the shear modulus of the equivalent poro-elastic skeleton, which is derived from the ultrasonic inversion is generally higher than the value obtained from low amplitude vibratory measurement. This is expected considering the dynamic modulus obtained from a poro-elastic material exhibits an increase with frequency, which is influenced by the frequency dependence of the loss factor [45].

7. Discussion

The resolution of the information (also referred to as sensitivity) on the length scale accessed by the ultrasonic waves of the measurement is closely related to the wavelength of the wave (it is usually a fraction of the wavelength). A rough estimate of the influence of the measuring frequency on the length scales assessed by the waves is determined by the characteristic frequency, f_c derived by Biot [25] and given as

$$f_c = \frac{\pi\mu}{4\rho_f a^2} \tag{17}$$

For frequencies above the characteristic frequencies, the Pouisville flow breaks down within the pores. For 1 MHz measuring frequency, the value of the pore size parameter can be estimated to be 0.8 μm. On this scale of observation, changes within the pore structure on length scales significantly smaller than the wavelength would be assigned to the skeleton. Thus changes in the gel porosity with time, which are typically associated with a length scale on the range of nano-meters, can only be indirectly inferred through changes in the skeleton properties. The water-filled space which allows continuous bulk flow of water on the scale of capillary pores can however be clearly delineated in the early age.

The influence of shrinkage on the measured parameters obtained from the inversion of the ultrasonic data requires careful

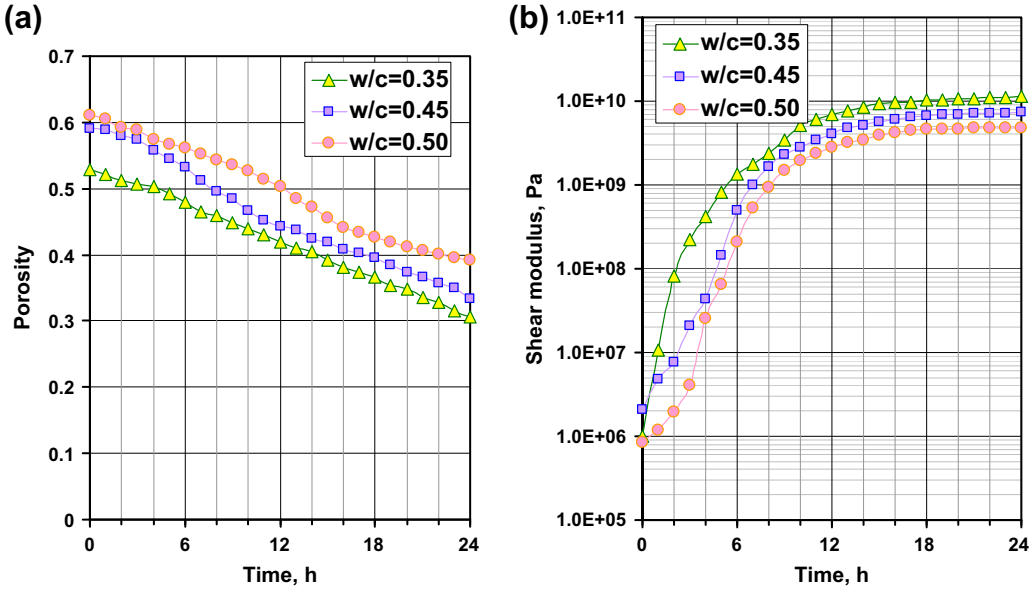

Fig. 6. Evolution of (a) porosity; and (b) shear modulus of solid skeleton.

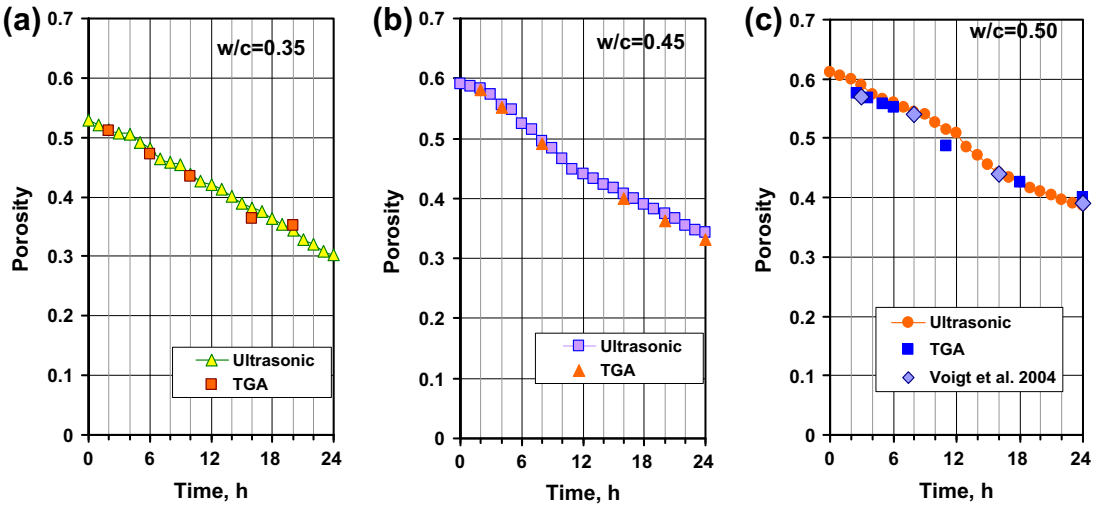

Fig. 7. Comparison between the porosity determined from the ultrasonic measurements and the thermogravimetric weight loss measurements: (a) $w/c = 0.35$; (b) $w/c = 0.45$; and (c) $w/c = 0.5$.

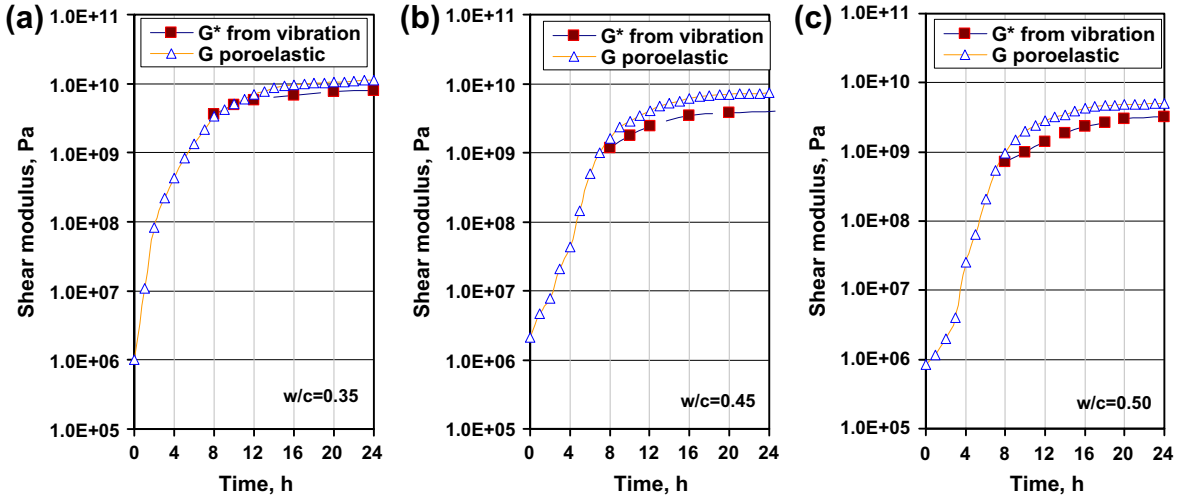

Fig. 8. Comparisons of shear moduli from poro-elastic inversion and vibration measurements for different w/c ratios: (a) $w/c = 0.35$; (b) $w/c = 0.45$; and (c) $w/c = 0.5$.

consideration. Autogenous shrinkage would result in a change in the macroscopic volume while chemical shrinkage produces changes within the structure of the paste. The potential influence of the shrinkage should be evaluated within the time frame of significance for changes in the capillary pore structure and the elastic modulus of the material. The shear modulus of hydrating cement pastes is known to evolve most rapidly (several orders of magnitude) in the first day of hydration [46]. There is a decrease in the rate with time and it is known to reach an asymptotic value after few days (7–10 days). Similarly significant changes in the capillary pore system have been shown to occur within the first few days of hydration [47]. Therefore, the significant period of interest is the first few days of hydration.

For a sealed system, since the total mass of the system remains constant, the change in volume results in a change in the bulk density. Considering the typical magnitude of autogenous shrinkage, which is typically on the order of 1000 με, changes in volume of the hydrating cement paste with age can be considered to produce insignificant changes in the bulk density of the material. In this early period, changes in the porosity and the elastic modulus of the hydrating cement paste occur on a significantly faster time scale than the corresponding change in density. The influence of changes in bulk density can therefore be treated as a second-order effect when compared to the corresponding change in the porosity of the system. This was verified by varying the bulk density used in the inversion within bounds associated with volume change due to autogenous shrinkage. There was an insignificant change in the values of the poro-elastic parameters obtained from the inversion when compared with the values predicted considering no change in the bulk modulus.

Chemical shrinkage is assessed from the decrease in volume of the products for a given volume of the reactants. Chemical shrinkage, may create air voids [48], which may influence the makeup of the hydration product. For low w/c ratio cement pastes, chemical shrinkage may also produce partial saturation in pores. In a saturated system, the additional water entering the unit volume may increase the density. Typical values of chemical shrinkage for completely hydrated cement paste are in the range of 5–7 ml/100 g of paste, which would result in a 7–8% internal reduction in volume [49]. For the lowest w/c ratio used in this study, $w/c = 0.35$, following the methodology presented by Hansen [5], the chemical shrinkage at 40% degree of hydration can be estimated to be approximately 5%. Considering some part of this 5% would manifest itself in the form of disconnected porosity, the effect of partial

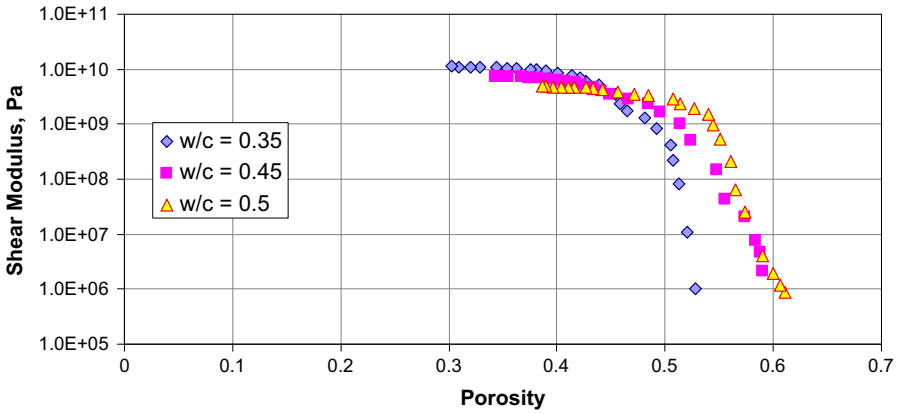

Fig. 9. Relationship between shear modulus and porosity for cement pastes with different *w*/*c* ratios.

saturation is insignificant. This effect may be come significant at later ages (with progressing hydration) or for *w*/*c* lower than 0.35 and would require careful consideration. Biot's model was primarily derived for fluid-saturated porous medium and with some modification can be adopted for a partially saturated medium.

The ultrasonic measurements provide a measure of porosity where relative movement is possible between the water and the solid skeleton. The water transport within cement is dominated by capillary pores when the capillary pore network is connected [50]. Therefore, capillary pore structure would play a significant role in determining the ultrasonic wave propagation in cement paste. Depercolated pores, if present, do not influence the movement of bulk water and would not influence the porosity determined from the ultrasonic measurements. Further, considering the length scales of resolution provided by the ultrasonic measurement, the depercolated pores within the solid matrix would be indirectly detected through their influence on the effective elastic property of the skeleton. It should be noted that very low *w*/*c* systems desaturate rapidly. In such systems, in addition to depercolation of pores, the influence of partial saturation should be considered in the poro-elastic representation.

The measurement of elastic properties obtained from the ultrasonic and vibration-based procedures correspond with the undrained condition, where the rate of stress application is significantly faster than the time scale associated with pressure decrease due to draining of the porous solid [51]. The quasi-static measurements on specimens with no confining pressure, on the other hand, approach the drained conditions. Measurements under undrained conditions include the effect from inertial and viscous interaction associated with relative fluid flow. The elastic moduli obtained from dynamic measurements (both ultrasonic and vibration) therefore exhibit frequency dependence and provide higher values than those obtained from the quasi-static measurements. It should be noted that any disconnected porosity within the solid matrix would influence the skeleton properties under both drained and undrained conditions identically.

It has been previously shown that the application of established relations such as the Kozeny–Carmen relations, which are suitable for use in rocks and other porous materials are not suitable for hardened cement paste. The reason is attributed to the very fine scale porosity in the form of gel pores, which do not contribute strongly to transport [52]. Early results by Powers et al. [53] indicated that when the capillary porosity decreases below a critical value, the permeability drops rapidly as the gel pores control the permeability. In this range it is reasonable to expect the Kozeny–Carmen relations not to work. However, in the early ages when capillary pores control the permeability, direct application of a proven relations in rocks have been found to provide reasonable estimates [52,42]. Extension of the proposed method as the capillary porosity decreases with progressing hydration requires careful consideration.

The results from the ultrasonic measurement can now be compiled to develop an understanding of the changes in the microstructure which produce setting and early strength gain in cement pastes. There are significant changes in shear modulus in the first few hours. Starting from a small value, there is an exponential increase in the shear modulus up to the end of the acceleration period, following which there is a noticeable change in the rate of increase. During the corresponding period there is a continuous decrease in the porosity and the trend indicates a slowing down in the rate with time. Changes in porosity are produced when the water is replaced with products of hydration. The formation of hydration products produces a larger relative increase in elastic modulus initially in the acceleration stage than later after setting. The sharp rise in the shear modulus, has previously been shown to indicate the emergence of a fully connected solid network of hydration products within the cement paste. This observation was first reported by Sayers and Dahlin [54] using through thickness ultrasonic propagation and later confirmed by Subramaniam and Wang [19] with rheological and ultrasonic reflection measurements. Following this, there is a very non-linear relationship between the pore structure densification (decrease in porosity) and shear modulus of the skeleton. The information on the evolution of porosity and the shear modulus can now be combined to directly understand the influence of structure formation and hydration on property development as shown in Fig. 9. The non-linear relationship between the porosity and shear modulus clearly depends upon the *w*/*c* ratio. This indicates the elastic modulus depends upon the initial porosity in addition to the porosity in the hydrating material. There is a larger relative increase in the shear modulus associated with a unit change of porosity for lower *w*/*c* ratios. This suggests that for a lower *w*/*c* ratio, because of the initial closer spacing of cement grains a smaller volume of hydration products produce a higher change in the shear modulus.

8. Conclusions

An ultrasonic method which measures the change in amplitude of horizontally polarized (SH) shear waves at the interface between fused-quartz and hydrating cement paste is presented. From the measured changes in the amplitude of the SH upon reflection, an equivalent poro-elastic material is derived. The shear modulus of the equivalent poro-elastic material is shown to compare favorably with the shear modulus of the cement paste obtained from vibration measurements. The porosity of the poro-elastic material

obtained from the ultrasonic measurements is shown to match the capillary porosity in cement paste obtained from the weight loss measurements using Power's model. Considering the results from the measurements, the following specific conclusions can be made:

1. The ultrasonic method provides for continuous, simultaneous measurement of capillary porosity and shear modulus of the material, with time. It can be used to track the development of microstructure and the mechanical properties of the skeleton composed of hydration products with time.
2. There are significant changes in shear modulus in the first few hours. There is an exponential increase in the shear modulus up to the end of the acceleration period, following which there is a noticeable change in the rate of increase. During the corresponding period there is a continuous decrease in the porosity, while the trend indicates a slowing in the rate of decrease.
3. There is a very non-linear relationship between the porosity and the increase in shear modulus in the first 24 h.

Appendix A

A.1. Reflection coefficient for SH wave at poro-elastic/elastic materials interface

Wave propagation through the porous medium is predicted by a pair of coupled displacement equations of motion governing both rotational and dilatational motions, obtained by combining the Biot's constitutive relationship and Darcy's law for flow through a porous medium [55]

$$\mu_b\nabla^2\vec{u} + (H - 2\mu_b)\nabla(\nabla\cdot\vec{u}) - C\nabla(\nabla\cdot\vec{w}) = \rho_b\ddot{\vec{u}} - \rho_f\ddot{\vec{w}} \tag{A1a}$$

$$C\nabla(\nabla\cdot\vec{u}) - M\nabla(\nabla\cdot\vec{w}) = \rho_f\ddot{\vec{u}} - m'\ddot{\vec{w}} - F\eta/\kappa\dot{w} \tag{A1b}$$

where $\vec{u} = \vec{u}(x,t)$ and $\vec{U} = \vec{U}(x,t)$ denote the average displacement of solid skeletal frame and the fluid, respectively, $\vec{w}(x,t) = \phi(\vec{u} - \vec{U})$ is the relative displacement of fluid and skeletal frame, ρ_b and ρ_f are bulk density of porous media and density of fluid respectively, κ is the coefficient of intrinsic permeability of the porous frame, $m' = c\rho_f/\phi$, c is the tortuosity coefficient (dimensionless parameter), which is a experimentally determined, ϕ is the porosity of porous media, $F(\omega, c, \eta)$ is a frequency correction function for the viscosity introduced by Biot which is considered as a complex function of the tortuosity c, angular frequency ω and fluid viscosity η [25,26]. In Eq. (A1) μ_b is the bulk shear modulus of the frame, H, C and M represent Biot's poro-elastic constants, which characterize the response of the composite [27] given as

$$H = \frac{(K_s - K_b)^2}{D_e - K_b} + K_b + \frac{4\mu_b}{3} \tag{A2a}$$

$$M = \frac{K_s^2}{D_e - K_b} \tag{A2b}$$

$$C = \frac{K_s(K_s - K_b)}{D_e - K_b} \tag{A2c}$$

where K_b is the bulk modulus of the skeletal frame (under drained conditions), $D_e = K_s\left(1 + \beta\frac{K_s}{K_f - 1}\right)$, K_s is the bulk modulus of the material of the skeletal frame and K_f is the bulk modulus of the pore fluid.

For a shear wave, the displacement vectors of the solid and the fluid phases could be written in terms of vector potentials as

$$\vec{u} = \nabla\times\vec{\varphi}_s \tag{A3a}$$

$$\vec{w} = \nabla\times\vec{\varphi}_f \tag{A3b}$$

The general form of the vector potentials is given as

$$\begin{cases}\vec{\varphi}_s = \varphi_s\exp[j(\omega t - \vec{k}^*_{sh}\cdot\vec{r})]\\ \vec{\varphi}_f = \varphi_f\exp[j(\omega t - \vec{k}^*_{sh}\cdot\vec{r})]\end{cases} \tag{A4}$$

where $\bar{r}$ is the position vector and $\bar{k}^*_{sh}$ is the complex wave number vector

Substituting (A4) into Eq. (A1), produces the frequency equation as shown below

$$\begin{cases}\mu_b k^{*2}_{sh}\varphi_s = \rho_b\omega^2\varphi_s - \rho_f\omega^2\varphi_f\\ (F\eta/\kappa)\omega\varphi_f = \rho_f\omega^2\varphi_s - m'\omega^2\varphi_f\end{cases} \tag{A5}$$

and the shear wave number is obtained as

$$k^*_{sh} = \left[\left(\rho_b\omega^2 - \frac{(\rho_f\omega^2)^2}{m'\omega^2 - j\omega(F\eta/\kappa)}\right)\Big/\bar{\mu}_b\right]^{1/2} \tag{A6}$$

where $\bar{\mu}_b$ represents the frequency dependent complex shear modulus of the skeleton frame and is obtained from the frequency transformation of μ_b given as

$$\bar{\mu}_b = \mu_b(1 + \delta_\mu j) \tag{A7}$$

where μ_b is the dynamic shear modulus of solid skeleton (drained condition), and the loss factor δ_μ, was introduced to consider the energy loss due to the friction among the phases of porous medium and is usually a small number in the range of 0.11–0.17 [27,56]. For most porous media, the function F in Eq. (A6) is given as [28]

$$F(\omega, c, \eta) = \left(1 + \frac{1}{2}j\omega\frac{\rho_f\kappa c}{\eta\phi}\right)^{1/2} \tag{A8}$$

An SH wave propagating in an elastic medium is incident at an angle θ to an interface with a poro-elastic material located at $z = 0$. The displacement potentials of the incident, reflected wave in the elastic medium and the transmitted wave in the poro-elastic medium are shown in Fig. A.1 and given below [27]

$$\varphi_i(x,z) = A_i\exp[j(\omega t - k_1\cos(\theta)z - k_c x)] \tag{A9a}$$

$$\varphi_r(x,z) = A_r\exp[j(\omega t + k_1\cos(\theta)z - k_c x)] \tag{A9b}$$

$$\varphi_{ts}(x,z) = A_{ts}\exp[j(\omega t - k^*_{sh}\cos(\alpha)z - k_c x)] \tag{A10}$$

$$\varphi_{tf}(x,z) = A_{tf}\exp[j(\omega t - k^*_{sh}\cos(\alpha)z - k_c x)] \tag{A11}$$

where k_1 and k^*_{sh} are the wave numbers in the elastic and poro-elastic materials respectively. Snell's law has been implicitly applied

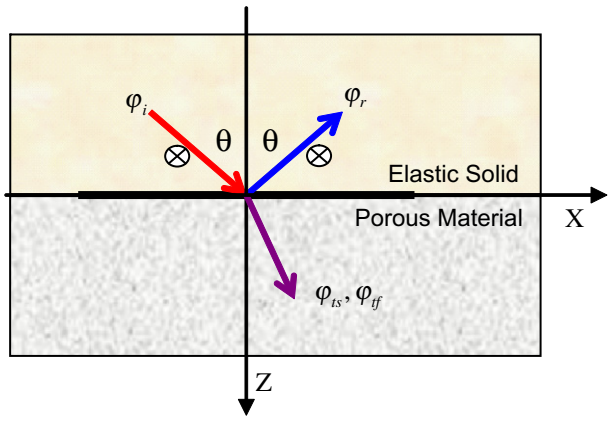

Fig. A.1. Reflection and refraction at interface between elastic and porous materials.

such that all the potentials which are generated at the interface give the same projection of the propagation vector on the interface.

$$k_{sh}^{*}\sin(\alpha) = k_1\sin(\theta) = k_c \tag{A12}$$

For a poro-elastic material with known properties (internal system variables are known), the exact magnitude of $r(f)$ after reflection can be obtained considering dynamic equilibrium and displacement continuity at the interface The boundary conditions at the interface, $z = 0$, are summarized as

(1) For the continuity of displacement

$$u_y\big|_{ealstic} = u_y\big|_{porous} \text{ or } \frac{\partial\varphi_i}{\partial z} + \frac{\partial\varphi_r}{\partial z} = \frac{\partial\varphi_{ts}}{\partial z} \tag{A13}$$

(2) For the equilibrium of tangential stress.

$$\tau_{yz}\big|_{ealstic} = \tau_{yz}\big|_{porous} \text{ or } \mu_1\left(\frac{\partial^2\varphi_i}{\partial z^2} + \frac{\partial^2\varphi_r}{\partial z^2}\right) = \bar{\mu}_b\frac{\partial^2\varphi_{ts}}{\partial z^2} \tag{A14}$$

where μ_1 is the shear modulus of the elastic material

(3) Continuity of fluid movement. It has the same boundary conditions with the previous case, and these conditions are satisfied automatically because of the characteristics of the SH wave mode.

By the combination of the above equations, the ratios of the amplitudes of the potentials $r^{*}(f)$ can be obtained as

$$r^{*}(f) = \frac{A_r}{A_i} = \frac{\bar{\mu}_b k_{sh}^{*}\cos(\alpha) - \mu_1 k_1\cos(\theta)}{\bar{\mu}_b k_{sh}^{*}\cos(\alpha) + \mu_1 k_1\cos(\theta)} \tag{A15}$$

References

[1] Thomas JJ, Jennings HM, Allen AJ. The surface area of hardened cement paste as measured by various techniques. Concr Sci Eng 1999;1:45–64.
[2] Jennings HM, Thomas JJ, Gevrenova JS, Constantinides G, Ulm FJ. A multi-technique investigation of the nanoporosity of cement paste. Cem Concr Res 2007;37(3):329–36.
[3] Juenger MCG, Lamour VHR, Monteiro PJM, Gartner EM, Denbeaux GPD. Direct observation of cement hydration by soft X-ray transmission microscopy. J Mater Sci Lett 2003;22(19):1335–7.
[4] Parrott LJ. Thermogravimetric and sorption studies of methanol exchange in alite paste. Cem Concr Res 1983;13(1):18–27.
[5] Hansen TC. Physical structure of hardened cement paste. A classical approach. Mater Struct 1986;19(6):423–36.
[6] Powers TC, Brownyard TL. Studies of the physical properties of hardened Portland cement paste. J Am Concr I 1947;18(8):972–90.
[7] Powers TC. Structure and physical properties of hardened Portland cement paste. J Am Ceram Soc 1958;41(1):1–6.
[8] Jennings HM, Bullard JW, Thomas JJ, Andrade JE, Chen JJ, Scherer GW. Characterization and modeling of pores and surfaces in cement paste: correlations to processing and properties. J Adv Concr Technol 2008;6(1):5–29.
[9] Fernandez MMC. Effect of particle size on the hydration kinetics and microstructural development of tricalcium silicate. Ph.D. thesis. École Polytechnique Federale De Lausanne; 2008.
[10] Sant G, Rajabipour F, Fishman P, Lura P, Weiss J. Electrical conductivity measurements in cement pastes at early ages: a discussion of the contribution of pore solution conductivity, volume, and connectivity to the overall electrical response. In: Reinhardt HW, editor. Advanced testing of fresh cementitious materials. Stuttgart, Germany; August 3–4, 2006.
[11] Bentz DP, Stutzman PE. Curing, hydration, and microstructure of cement paste. ACI Mater J 2006;103(5):348–56.
[12] Bentz DP, Garboczi EJ. Percolation of phases in a three-dimensional cement paste microstructural model. Cem Concr Res 1991;21:325–44.
[13] Ye G, van Breugel K, Fraaij ALA. Experimental study and numerical simulation on the formation of microstructure in cementitious materials at early age. Cem Concr Res 2003;33(2):233–9.
[14] Chotard TJ, Boncoeur-Martel MP, Smith A, Dupuy GP, Gault C. Application of X-ray computed tomography to characterise the early hydration of calcium aluminate cement. Cem Concr Compos 2003;25(1):145–52.
[15] Subramaniam KV, Lee J, Christensen BJ. Monitoring the setting behavior of cementitious materials using one-sided ultrasonic measurements. Cem Concr Res 2005;35(5):850–7.
[16] Voigt T, Shah SP. Properties of early-age Portland cement mortar monitored with shear wave reflection method. ACI Mater J 2004;101(6):473–82.
[17] Wang X, Subramaniam KV, Lin F. Ultrasonic measurement of viscoelastic shear modulus development in hydrating cement paste. Ultrasonics 2010;50(7):726–38.
[18] Akkaya Y, Voigt T, Subramaniam KV, Shah SP. Nondestructive measurement of concrete strength by an ultrasonic wave reflection method. Mater Struct 2003;36(262):507–14.
[19] Subramaniam KV, Wang X. An investigation of microstructure evolution in hydrating cement paste through setting using ultrasonic and rheological measurements. Cem Concr Res 2010;40(1):33–44.
[20] Pichler C, Lackner R, Mang HA. A multiscale micromechanics model for the autogenous-shrinkage deformation of early-age cement-based materials. Eng Fract Mech 2007;74(1–2):34–58.
[21] Ulm FJ, Constantinides G, Heukamp FH. Is concrete a poromechanics material? A multiscale investigation of poroelastic properties. Mater Struct 2004;37(265):43–58.
[22] Bernard O, Ulm FJ, Lemarchand E. A multiscale micromechanics-hydration model for the early-age elastic properties of cement-based materials. Cem Concr Res 2003;33(9):1293–309.
[23] Lin F, Meyer C. Modeling shrinkage of Portland cement paste. ACI Mater J 2008;105(3):302.
[24] Coussy O. Poromechanics. West Sussex, England: Wiley; 2004.
[25] Biot M. Theory of propagation of elastic waves in a fluid-saturated porous solid. I. Low-frequency range. J Acoust Soc Am 1956;28(2):168–78.
[26] Biot M. Theory of propagation of elastic waves in a fluid-saturated porous solid. II. Higher frequency range. J Acoust Soc Am 1956;28(2):179–91.
[27] Stoll RD, Kan TK. Reflection of acoustic-waves at a water–sediment interface. J Acoust Soc Am 1981;70(1):149–56.
[28] Albert DG. A comparison between wave-propagation in water-saturated and air-saturated porous materials. J Appl Phys 1993;73(1):28–36.
[29] Zimmerman C, Stern M. Analytical solutions for harmonic wave propagation in poroelastic media. J Eng Mech-ASCE 1994;120(10):2154–78.
[30] Johnson DL, Plona T. Acoustic slow waves and the consolidation transition. J Acoust Soc Am 1982;72(2):556–65.
[31] Chotiros NP. An inversion for Biot parameters in water-saturated sand. J Acoust Soc Am 2002;112(5):1853–68.
[32] Deresiewicz H, Skalak R. On uniqueness in dynamic poroelasticity. B Seismol Soc Am 1963;53(4):783–9.
[33] Gurevich B, Schoenberg M. Interface conditions for Blot's equations of poroelasticity. J Acoust Soc Am 1999;105(5):2585–9.
[34] Alig I, Lellinger D, Sulimma J, Tadjbakhsch S. Ultrasonic shear wave reflection method for measurements of the viscoelastic properties of polymer films. Rev Sci Instrum 1997;68(3):1536–42.
[35] Williams D, Saak A, Jennings HM. The influence of mixing on the rheology of fresh cement paste. Cem Concr Res 1999;29(9):1491–6.
[36] Achenbach JD, Komsky IN, Lee YC, Angel YC. Self-calibrating ultrasonic technique for crack depth measurement. J Nondestruct Eval 1992;11(2):103–8.
[37] Subramaniam KV, Mohsen JP, Shaw CK, Shah SP. Ultrasonic technique for monitoring concrete strength gain at early age. ACI Mater J 2002;99(5):458–62.
[38] Taylor HFW, Portland cement: hydration products. In: Roy D, editor. Instructional modules in cement science, a publication of materials education council. PA: Materials Research Laboratory University Park; 1985.
[39] Subramaniam KV, Popovics JS, Shah SP. Determining elastic properties of concrete using vibrational resonance frequencies of standard test cylinders. Cem Concr Aggr 2000;22(2):81–9.
[40] Berryman J. Confirmation of Biot's theory. Appl Phys Lett 1980;37(4):382–4.
[41] Plona T. Observation of a second bulk compressional wave in a porous medium at ultrasonic frequencies. Appl Phys Lett 1980;36(4):259–61.
[42] Cui L, Cahyadi JH. Permeability and pore structure of OPC paste. Cem Concr Res 2001;31:277–82.
[43] Mindess S, Young JF. Concrete. Englewood Cliffs, NJ: Prentice Hall; 1981. p. 76–80.
[44] Voigt T. The application of an ultrasonic shear wave reflection method for nondestructive testing of cement-based materials at early age. PhD thesis. Germany: University of Leipzig; 2004.
[45] Park J. Measurements of the frame acoustic properties of porous and granular materials. J Acoust Soc Am 2005;118(6):3483–90.
[46] Boumiz A, Sorrentino D, Vernet C, Cohen Tenoudji F. Modelling the development of the elastic moduli as a function of the hydration degree of cement pastes and mortars. In: Nonat A, editor. Proceedings 2nd international RILEM symposium, hydration and setting, RILEM, Cachan Cedex, France; 2000. p. 295–316.
[47] Consolati G, Quasso F. Evolution of porosity in a Portland cement paste studied through positron annihilation lifetime spectroscopy. Radiat Phys Chem 2003;68:519–21.
[48] Tazawa E, Miyazawa S, Kasai T. Chemical shrinkage and autogenous shrinkage of hydrating cement paste. Cem Concr Res 1995;25(2):288–92.
[49] Geiker M, Knudsen T. Chemical shrinkage of Portland cement pastes. Cem Concr Res 1982;12(5):603–10.
[50] Ye G. Percolation of capillary pores in hardening cement pastes. Cem Concr Res 2005;35:167–76.
[51] Sanahuja J, Dormeiux L, Chanvillar G. Modelling elasticity of a hydrating cement paste. Cem Concr Res 2007;37:1427–39.
[52] Christensen BJ, Mason TO, Jennings HM. Comparison of measured and calculated permeabilities for hardened cement paste. Cem Concr Res 1996;26(9):1325–34.

[53] Powers TC, Copeland LE, Mann HM. Capillary continuity or discontinuity in cement pastes. J Portland Cem Assoc Res Dev Lab 1959;10:38–48.
[54] Sayers CM, Dahlin A. Propagation of ultrasound through hydrating cement pastes at early times. Adv Cem Based Mater 1993;1(1):12–21.
[55] Biot M. Mechanics of deformation and acoustic propagation in porous media. J Appl Phys 1962;33(4):1482–98.
[56] Chotiros NP. Biot model of sound propagation in water-saturated sand. J Acoust Soc Am 1995;97(1):199–214.